Nature Environment and Pollution Technology
An International Quarterly Scientific Journal

p-ISSN: 0972-6268
(Print copies up to 2016)
e-ISSN: 2395-3454

Vol. 24 | No. 2 | Article ID D1714 | 2025

Original Research Paper

https://doi.org/10.46488/NEPT.2025.v24i02.D1714

Open Access Journal

Changes in Land Use Land Cover and its Resultant Impacts on the Urban Thermal Environment of Chattogram City: A Spatio-Temporal Analysis Based on Remote Sensing and GIS Techniques

Sagar Mozumder, Mahfuza Parveen† and A.B.M. Kamal Pasha
Department of Environmental Science and Disaster Management, Daffodil International University, Dhaka, Bangladesh
†Corresponding author: Mahfuza Parveen; mahfuza.esdm@diu.edu.bd

Abbreviation: Nat. Env. & Poll. Technol.
Website: www.neptjournal.com

Received: 12-08-2024
Revised: 23-09-2024
Accepted: 19-10-2024

Key Words:

Land use and land cover
Landsat
Land surface temperature
Probability matrix
Transition matrix
Urban heat island

Citation for the Paper:

Mozumder, S., Parveen, M. and Pasha, A.B.M.K., 2025. Changes in land use land cover and its resultant impacts on the urban thermal environment of Chattogram City: A spatio-temporal analysis based on remote sensing and GIS techniques. *Nature Environment and Pollution Technology*, 24(2), p. D1714. https://doi.org/10.46488/NEPT.2025.v24i02.D1714

Note: From year 2025, the journal uses Article ID instead of page numbers in citation of the published articles.

ABSTRACT

The present study assessed the changes in land use and land cover to correlate the variations in the land surface temperature of Chattogram City. To analyze land use land cover (LULC) change and determine its effects on land surface temperature in the city area, temporal Landsat (5,7 ETM+ and 8,9 OLI) imageries from four time periods (2007, 2012, 2017, and 2022) were used. To assess the correctness of the picked random pixels, current ground truth data gathered from several sources was applied. Raster data has been utilized to identify the places that are influenced year-round in the green space (i.e., vegetation cover) and to examine the remote sensing image categorization for the green area using satellite images. These enable the study to explain the causes of the degradation and alteration of green space throughout time. The study identified that urbanization has resulted in a significant rise (about 2840 hectares, 16.74%) in urban land between 2007 and 2022, causing a loss of vegetative land (about 656 hectares, 3.85%). Additionally, the research concentrated on the actual affected area and attempted to forecast the cities' land use in 2037, which revealed a large loss of vegetation by that year. The research has the potential to be utilized as a reference in the future.

INTRODUCTION

The land is a crucial resource and a source of livelihood. It is an essential and limited resource for some most essential human activities, including agriculture, manufacturing, forestry, energy generation, settlement, recreation, and water catchments and storage. Land is a key component of production, and for a large portion of human history, economic development has been closely correlated with it. It includes biophysical characteristics, including terrain, geology, hydrology, biodiversity, soil, and topography (Gaonkar et al. 2024). Another definition of land includes socioeconomic elements like management and technology, and land use refers to how and why people use the land and its resources (Meyer 1995). In general, a piece of land is modified when its use changes. This shift is driven by needs, which need not just change the land cover but also its intensity and management (Verburg et al. 2000). Agricultural expansion, propelled by population increase and technical progress, has profoundly transformed land cover, especially in developing nations, eclipsing other influences such as urbanization and deforestation (Kirkpatrick 2024). Social structure, attitudes, and values have all changed significantly in the same period. Urban regions are thought to be the most dynamic areas on the surface of the Earth, according to the history of urban growth. Urbanization has a significant negative influence on the local ecosystem (Pasha et al. 2018) despite its relevance to the regional economy (Saraswat et al. 2024). Only 14% of the world's population lived in urban areas in 1900; by 2000, this percentage had risen to 47%, which has recently touched 56% (Ritchie &

Roser 2018, Long et al. 2007). Almost all nations around the globe experience urban expansion. However, the rate of growth varies. Urban environment and ecology are currently the main environmental issues that require rigorous analysis and monitoring to effectively regulate land use. Inventories of land usage and land cover are becoming more and more important in a variety of fields, including agricultural planning, urban planning, and infrastructure development (Kavitha et al. 2021). Other forms of land use turning into urban land can be characterized as the primary change in land use in these locations. Several elements, including both physical and human aspects, have an impact on the intricate process of land use change in major urban areas. On the one hand, socioeconomic reasons are typically linked to and responsible for accelerated urban growth; on the other, the process of urbanization has a significant impact on the local economy (Tyagi et al. 2023).

One way to learn about urban environments is through remote sensing, which is also a crucial tool for comprehending and addressing many issues that face cities and their suburbs. (Lillesand et al. 2015). Change detection is crucial because it enables the researcher to comprehend and track the pattern of land cover change in the study area (such as urbanization, deforestation, and agricultural land management) (Ahmed 2011). The remote sensing technique is a great data source from which updated information and changes in land use and land cover (LULC) can be effectively extracted, examined, and simulated. A lot of pressure has been put on the nearby land and its biotic and abiotic resources in recent decades due to developing countries' rapid urbanization and population increase (Singh & Singh 2023). This pressure is also the cause of the urban areas accelerating rate of landscape change. Numerous studies have demonstrated that the land cover change brought on by urbanization has a significant impact on the radiative, thermodynamic, and hydrological processes that can modify the local climate (Qian et al. 2022). The quality of vegetation cover reduces its ability to moderate temperature patterns, resulting in a negative correlation between vegetation and land surface temperature (Fatemi & Narangifard 2019). One of the biggest issues of this century is the urban heat island (UHI), which is a product of human civilization's urbanization and industrialization (Jabbar et al. 2023). The rise in surface temperature caused by human activity can be a major cause for the development of urban heat islands, which is one of the most significant markers of urbanization. Urban heat island (UHI) is a problem that results from the unchecked urbanization of areas (Karakuş 2019). Because of the significant amount of vegetation loss, urban growth, and shifting of forest land to agricultural the, the land surface temperature increases, which ultimately develops UHI (Thomas et al. 2024). After urbanization, it is impossible to restore the forest and vegetation to their pre-urban state (Mia et al. 2017). By the end of 2047, it is predicted that urban migration will account for 50% of all migration.

Bangladesh is one of the most populous nations in the world and is currently developing. It has recently experienced major environmental degradation and rapid, uncontrolled urban growth. However, because of rapid urbanization, the region has seen significant environmental degradation and several ecological issues, including deforestation, biodiversity loss, soil erosion, and modifications to the carbon sink in water-based ecosystems (Thomas et al. 2024). Chattogram is the second largest city of Bangladesh which is also experiencing land use and land cover changes because of urban development.

The local and microclimate of Chattogram City have changed as a result of anthropogenic activities and urban growth, which are driven by land use, such as built-up areas, impermeable structures, industrial activities, waste dumping, nucleated high buildings, and transportation activities (Pathirana et al. 2014). New urban development in the metropolis is destroying urban trees and plants, which are crucial for protecting the urban ecosystem and environment. With a population of 66% living in urban areas, Chattogram, Bangladesh's second-largest city and business hub, is currently one of the fastest-growing cities in the world. It accounts for 19.7% of the country's urban population and 30% of the GDP (Hassan & Nazem 2016). The urban forests, water bodies, and vegetation in cities have all been gradually destroyed by the rapid rise of urbanization in Chattogram City (Gazi et al. 2021). It is important to take into account Chattogram, a developing city in Bangladesh when analyzing LST in connection to land-use change. Therefore, it is essential to recognize how LST is changing in Chattogram City. According to a (BBS 2011) analysis, the country is losing 809 km2 of agricultural land every year as a result of city growth, road construction, and infrastructure development. Due to migration from rural to urban areas, Chattogram City's average annual growth rate has reached 17.5% (Mia et al. 2015). Since rising urbanization has a negative effect on LST (Hokao et al. 2012), it is critical to track changes in land use and land cover and how they relate to LST behavior in Chattogram. Hence, the present study aimed to identify the rate of changes in land use and land cover in the study area. Moreover, the study investigated the multitemporal spatial dynamics of LULC change and its contribution to UHI generation for Chattogram City. Additionally, it determined the mean LST for each LULC class, the dynamics of change, and the relation with the urban landscape. This study used open-source Landsat imageries

with advanced remote sensing and GIS technology to trace the dynamics of urban growth, monitor geographical and temporal changes in land use and land cover, and evaluate Chattogram's environmental sustainability.

MATERIALS AND METHODS

The Study Area

The city of Chattogram, which is part of the Chattogram district, is bordered by rivers and is made up of small hills and narrow valleys. In addition to being Bangladesh's busiest seaport, Chattogram is also renowned as the country's commercial center. The second-largest city in Bangladesh is Chattogram, with a land area of 157 km^2 (Mia et al. 2015). The city is located between latitudes 21°54′ and 22°59′ north and 91°17′ and 92°14′ east. Its southern and eastern boundaries are formed by the Karnaphuli River, northern and eastern by the Halda River, and western by the Bay of Bengal. Chattogram City is the chosen research topic for this study because it has expanded its urban zone with time and become the second most important city after the capital. (Fig. 1). About 2.5 million people live in the city, which is under the control of the City Corporation, and it covers an area of about 168 square kilometers (Statistics 2011). Approximately 40% of the nation's large-scale enterprises are located in Chattogram, which also accounts for 85% of Bangladesh's imports and 80% of its exports in the country's seaborne trade (Hassan & Nazem 2016), which makes it an important location for this study.

Classification of Images

Satellite imagery is detailed and essential for supplying geographic information. The complexity of field labor and study time is reduced by the quantitative and qualitative data provided by satellite and remote sensing imagery (Shahbaz et al. 2012). Image Classification is one of the most efficient methods that can provide both qualitative and quantitative data (Vaiphasa et al. 2011). Supervised image classification

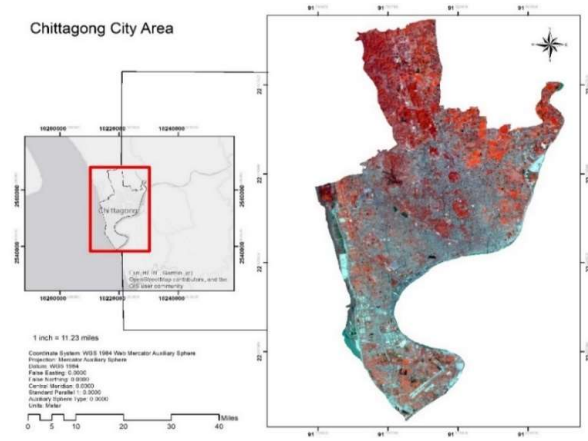

Fig. 1: The location of Chattogram City selected for the present study.

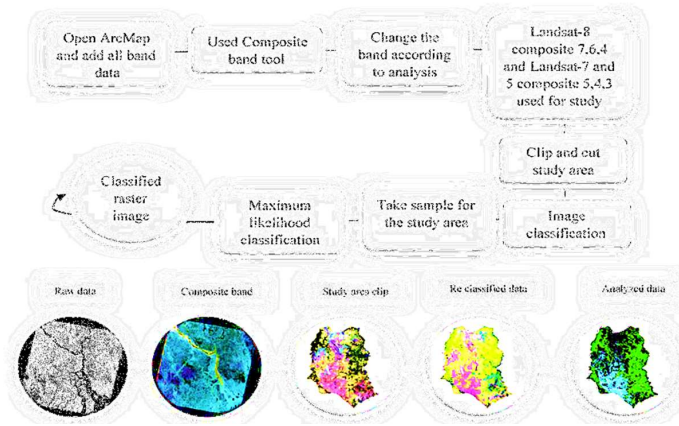

Fig. 2: Representation of Data analysis process.

is the method (Fig. 2) used here to identify and calculate the land cover amount of the study area. In this process researcher manually inputs some supervised samples in ArcGis software (Fig. 2). Later, the software itself calculates the pixel of the image data and shows the output (Abburu & Golla 2015). The amount of land cover used in an area can be calculated with the help of production. In this case, the land cover shows the amount of increase or decrease meant for a particular land cover category.

Markov Modeling for Probability Matrix

A Markovian process uses the current state of a system to predict its future state over time using the same design. Depending on the status right now, it is a random procedure. Markov chain is a discrete-time stochastic process (Winston & Goldberg 2004). Here, the condition of the future can be determined by analyzing the present state of that individual area (Ross 2014). Markovian property can be described and stated with

$$i_0, i_1, \ldots, i_{t-1}, i_t, i_{t+1}, and\ all\ t \geq 0$$

$$P(x_{t+1} = i_{t+1} \mid x_t = i_t, x_{t-1} = i_{t-1}, \ldots., x_1 = i_1, x_0 = i_0) = P(x_{t+1} = i_{t+1} \mid x_t = i_t \quad \ldots(1)$$

According to the Markov chain, it assumes that the conditional probability does not change over time. For all States i and j and all t, $P(x_{(t+1)} = j|x_t = i)$ is independent of , as expressed in Eq (1)

$$P(x_{t+1} = j \mid x_t = i) = p_{ij} \quad \ldots(2)$$

Where, P_{ij} = Transition probability that, given the system is in State i at time t, It will be in a state j at the time $(t + 1)$. The transition probabilities are expressed as a $[m \times m]$ Matrix and it is called the transition probability matrix or transition matrix, P. The characteristics of the transition probability matrix as p are given below

$$P = \begin{bmatrix} p_{11} & p_{12} \cdots & p_{1m} \\ p_{21} & p_{22} \cdots & p_{2m} \\ p_{m1} & p_{m2} \cdots & p_{mm} \end{bmatrix} \quad \ldots(3)$$

The estimation of transition probabilities in a Markov chain-based deterioration model requires data from the condition assessments of existing systems. (Baik et al. 2006).

Calculation of NDVI

The amount of vegetation or biomass present in the environment is measured by the Normalized Difference Vegetation Index (NDVI). Greater greenness and healthy vegetation are indicated by a higher NDVI (Curran 1980). Data from Landsat MSS and TM can be used to calculate NDVI (Jensen 1996). The reflectance data from the red (red) and near-infrared (nir) bands were utilized to calculate the NDVI values for the research area (Tan et al. 2010).

$$NDVI = (\rho_{nir} - \rho_{red})/(\rho_{nir} + \rho_{red}) \quad \ldots(4)$$

Land Surface Temperature (LST) for Landsat 8/9 and 7/5 Image

The temperature that is sensed while touching the ground in a region is known as the land surface temperature. It is distinct from the temperature of the air or the atmosphere. Different Landsat data sets, including Landsat-9, 8, 7, and Landsat-5, were employed in this investigation (Pasha et al. 2023). Because the two Landsat data have different band values, calculating the land surface temperature for the two sets of data is different. There are eleven bands available for Landsat 8 and 9, and we used band 10 TIRS to calculate LST (Fig. 3) (Avdan & Jovanovska 2016). Thermal mapping is done using the Landsat 8 data band-10 TIRS, which specifies the thermal band with a 100-meter precision. Similar to this, Landsat 4-5 has a total of seven bands, each of which denotes a separate class. The thermal infrared band in Landsat 4-5 is band number 6, and it is frequently used to determine an area's thermal mapping (Fig. 3) (Qin et al. 2001). Software named Arc GIS 10.4 has been used to perform the calculation. In order to obtain the LST, specific formulas were utilized in the raster calculator.

For Landsat 8/9, to recover the land surface temperature of various years from satellite photos, an image-based methodology has been used (Lo & Quattrochi 2003). OLI images were converted using the USGS standard equation, and the DNs of the TIR bands of each year's ETM images were transformed to spectral radiance (Fig. 3) using the method employed by Chander et al. (2009).

The algorithm's initial stage is the input of Band 10, which is used to calculate the atmospheric Spectral Radiance (Fig. 3). The program retrieves the top of atmospheric (TOA) spectral radiance (Lλ) once Band 10 is inputted in the background using calculations from the USGS website.

$$L\lambda = M_L * Q_{cal} + A_L - O_i \quad \ldots(5)$$

Where ML stands for the band-specific multiplicative rescaling factor, Qcal for the Band 10 image, AL for the Band 10 additive rescaling factor, and Oi for the Band 10 correction (Barsi et al. 2014).

The next step is to calculate and convert spectral radiance to Brightness temperature (BT) by using metadata (Fig. 3) where. Using the thermal constants provided in the metadata file, the TIRS band data should be changed from spectral radiance to brightness temperature (BT) after being converted from digital numbers (DNs) to reflection.

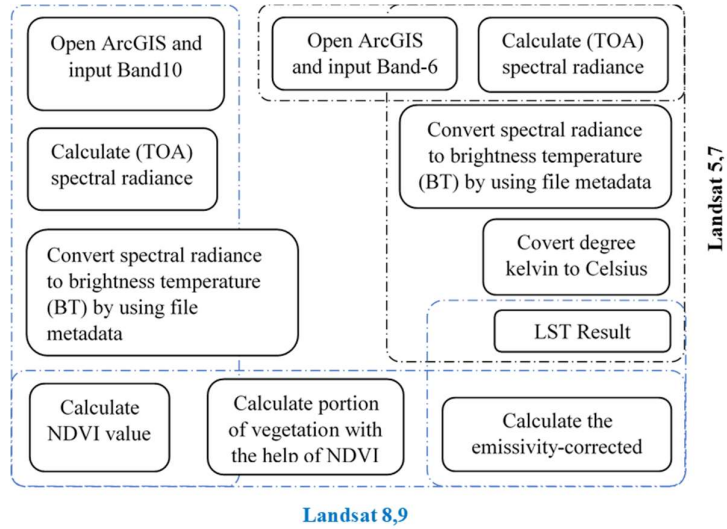

Fig. 3: Graphical representation of the calculation of LST from Landsat 8,9 and 5,7 satellite images.

The tool's algorithm converts reflectance to BT using the equation shown below,

$$BT = \frac{K_2}{\ln\left[\left(\frac{K_1}{L_\lambda}\right)+1\right]} - 273.15 \quad \ldots(6)$$

Where K1 and K2 refer to the metadata's band-specific thermal conversion constants, the radiant temperature is corrected by adding absolute zero (about -273.15°C) to obtain the fiugres in Celsius (Xu & Chen 2004). The Thermal constant for Landsat 9, Band 10 image is used in the method. Where the value of $K_{1\ (Constant\ Band\_10)}$ is 799.0284, and the value of $K_{2\ (Constant\ Band\_10)}$ is 1329.2405. For the Rescaling factor for Landsat 9, Band 10 image, the value of $M_{L\ (Radiance\ Mult\ Band)}$ is 0.000384 also, the value of $A_{L\ (Radiance\ Add\ Band)}$ is 0.10000, and the Correction value of Band 10 is $O_i = 0.29$.

In the third step NDVI value needed to be calculated following the procedure in section (2.5) then the portion of Vegetation P_v is calculated. The NDVI values for vegetation and soil ($NDVI_v = 0.5$ and $NDVI_s = 0.2$) are suggested to be used under global settings for computing P_v (Sobrino et al. 2004).

Where,

$$P_v = \left(\frac{NDVI - NDVI_s}{NDVI_v - NDVI_s}\right)^2 \quad \ldots(7)$$

However, the figure for vegetated surfaces, 0.5, may be too low because the NDVI values vary for each place. Since NDVIV and NDVIs will rely on atmospheric conditions, it would not be possible to establish global values in the case of an NDVI computed using TOA reflectivities (Fig. 3). Global values from NDVI can be obtained from at-surface reflectivities (Jiménez-Muñoz et al. 2009).

In the next phase, surface emissivity has to be calculated to estimate LST. The land surface emissivity (LSE) must be known because it is a proportionality factor that scales blackbody radiance (Planck's law) to forecast emitted radiance and measures how effectively thermal energy is transmitted from the surface to the atmosphere (Jiménez-Muñoz et al. 2006). The emissivity can be calculated with the following formula (Sobrino et al. 2004).

$$\varepsilon\lambda = \varepsilon_{v\lambda} P_v + \varepsilon_{s\lambda}(1 - P_v) + C_\lambda \quad \ldots(8)$$

Where, C stands for surface roughness (C = 0 for homogeneous and flat surfaces) and is constant at 0.005 for vegetation and soil emissivities, respectively (Sobrino & Raissouni 2000).

As a final step, the land surface temperature T_s, also known as the emissivity-corrected land surface temperature, is determined as follows.

$$T_s = \frac{BT}{\left\{1 + \left[\left(\frac{\lambda BT}{\rho}\right)\ln \varepsilon_\lambda\right]\right\}} \quad \ldots(9)$$

Where Ts is the LST in degrees Celsius (C), BT is the at-sensor BT (C), is the emission wavelength (for which the maximum response and the average of the limiting wavelength (= 10.895) will be used), and is the previously determined emissivity (Markham & Barker 1985).

For Landsat 7 and 5 images, L_λ has to be calculated with the following formula,

$$L_\lambda = L_{min} + \frac{L_{max} - L_{min}}{QCAL_{max} - QCAL_{min}}(DN - QCAL_{min}) \quad \ldots(10)$$

Qcal is the DN of each image in the metadata of Landsat 7 and 5, $QCAL_{max}$ is the maximum DN (255), and $QCAL_{min}$ is the minimum DN (1). The top of the atmosphere (TOA)

radiances, L_{max} and L_{min}, are scaled to $QCAL_{max}$ and $QCAL_{min}$ in W/(m^2 srm), respectively. Using the following equation, the radiant images were transformed from the DNs to the spectral radiance to determine the blackbody temperature.

$$T_b = \frac{K_2}{\ln\left\{\left(K_1/L_\lambda\right)+1\right\}} \quad \ldots(11)$$

Where K_1 and K_2 are prelaunch calibration constants in Kelvin units acquired from the image metadata file, T_b is the effective at-sensor brightness temperature in Kelvin units, L is spectral radiance in W/(m^2 srm), For the Thermal constant for Landsat 7, Band 6 image is, $K_{1\ (Constant\ Band\ 6)\ =}$ 666.09 and the $K_{2\ (Constant\ Band\ 6)=}$ 1282.71. The Rescaling factor for Landsat 7 and 5, Band 6 image is $QUANTIZE_{\ Cal\ Max\ Band\_6=}$ 255 and $QUANTIZE_{\ Cal\ Min\ Band\_6=}$ 1.

The calculated LST values were then translated to the standard Degree Celsius (°C) unit by subtracting the absolute zero, which is roughly minus 273.5°C (Xu & Chen 2004).

$$LST = T_b - 273.15 \quad \ldots(12)$$

Model Accuracy, Assumptions, and Potential Errors

Rooted on the land use land cover changes data from 2007 to 2022, the Markov model anticipates land use changes depending upon the prior patterns in the future, which is likely to be a fallacy. It, however, does not, out of consideration, include the irregular events that can occur, such as a change in policy and natural catastrophes, among others, and simplifies changes to be linear, which may not adequately portray the complexities related to urban growth. In this case, present conditions and the quality of data used for forecasting predictions, as well as the fact that the transition probabilities do not change, are major factors in determining the predictive power of these matrices. The span or the window of the data, which, in this instance, is 15 years of history, makes it difficult to trust the forecasting, for it is prone to future incongruence with present trends. The expected figures for urban encroachment and vegetation destruction relate to other fast-developing cities like Dhaka and Kolkata. These comparisons do enhance the forecasts made by the model, but their usage carries risks and should thus be moderated. The Markov modeling framework does not incorporate sudden land cover changes or any effects of land cover change on land use. This development could be even more beneficial for future projections by adding some innovative models with more dynamics, like the CA-Markov model, and integrating socio-economical and environmental factors in the modeling process.

RESULTS

Changes in Land Use and Land Cover from 2007 to 2022

This study showed the land use and land cover of the Chattogram City Area. According to the analysis of land use and land cover, only 5901.21 hectares of urban area were found in 2007 (Table 1). However, it expanded significantly from 5901.21 ha in 2007 to 6895.08 ha in 2012, rising from 34.77% to 40.63% of the total study area during those five years (Fig. 4). In 2017, the urban area's growth trends accounted for 8073.36 ha, or 47.57% of the total area (Table 1). The Chattogram city has a huge population, and the urban area is growing swiftly**.** The urban area has grown even more, accounting for 8741.52 ha in 2022, or 51.51% of the city's total land area (Table 1). But as the graph demonstrates, there has been a significant decline in the vegetation cover, with 0.4% (70 ha) between 2007 and 2012 and 2.15% (363.51 ha) between 2012 and 2017. 1.3% (220.95 acres) of vegetation was lost between 2017 and 2022 (Fig. 4). Over 15 years, 654.39 ha less land was covered by vegetation. These trends in plant loss should worry city people because they portend an increase in urban heat, which is harmful to both the environment and human civilization. There was a discernible drop in bare land, agricultural land, and water body area. Agriculture occupied 3641.54 hectares (21.46%) of the total area in 2007, increased to 4686.03 ha (27.63%) in 2012, and again decreased to 2733.3 ha (16.11%) in 2017 (Table 1). According to the study, the total amount of agricultural land decreased by 908.64 ha between 2007 and 2017, but in 2022, it climbed by roughly 5%, or 3661.74 ha, of the study region's total land cover (Table 1). The area's bare land severely declined from 3215.07ha to 1793.07ha between 2007 and 2012 (a loss of 8.38%), but it dramatically increased from 2012 to 2017 (a gain of 8.15%) and became 3176.82 ha. The total land area in 2022 was 1574.1 ha, a 9.44% decrease in bare land area (Table 1). Over the course of 15 years, bare land dropped by 1640.97 ha in total. The area occupied by inland water bodies shrunk between 2007 and 2012, from 1196.28 hectares in 2007 to 650.25 ha in 2012, and it also shrunk significantly between 2012 and 2017, between 650.25 hectares in 2012 and 404.46 hectares in 2017 (Table 1). It did, however, grow in 2022, though still only by 3.72% of the overall area. Between 2007 and 2017, the water body shrunk by 791.82 ha, while between 2017 and 2022, it grew by 227.07 ha (Table 1). Even though the total area by the years 2007, 2012, 2017, and 2022 was almost the same, the internal land use and landcover types have changed dramatically (Fig. 4 & 5). Urban lands produce more urban heat island zones than other types of land use.

Table 1: Land cover change from 2007 to 2022.

Class	Hectors	P%	Hectors	P%	Hectors	P%	Hectors	P%
	2007		2012		2017		2022	
Vegetation	3015.9	17.77%	2945.97	17.36%	2582.46	15.22%	2361.51	13.92%
Agriculture	3641.94	21.46%	4686.03	27.61%	2733.3	16.11%	3661.74	21.58%
Urban	5901.21	34.77%	6895.08	40.63%	8073.36	47.57%	8741.52	51.51%
Bare land	3215.07	18.95%	1793.07	10.57%	3176.82	18.72%	1574.1	9.28%
Water body area	1196.28	7.05%	650.25	3.83%	404.46	2.38%	631.53	3.72%
Total	16970.4	100%	16970.4	100%	16970.4	100%	16970.4	100%

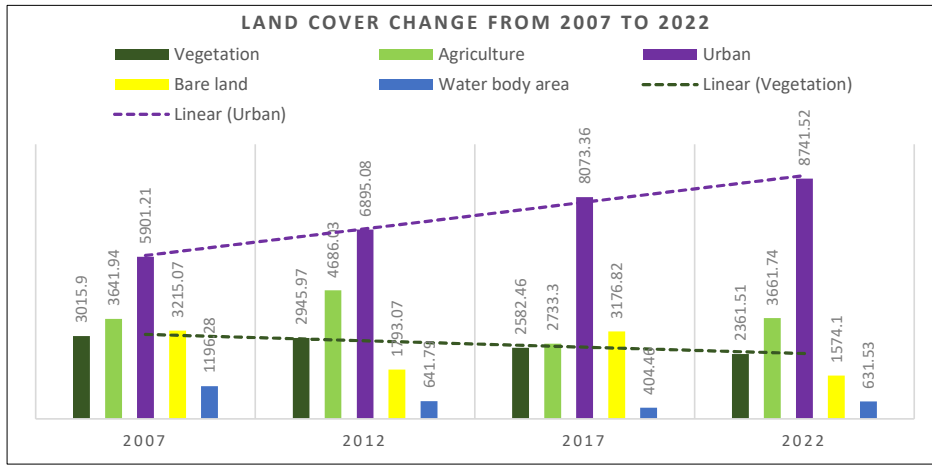

Fig. 4: Land cover change, including vegetation and urban trend line.

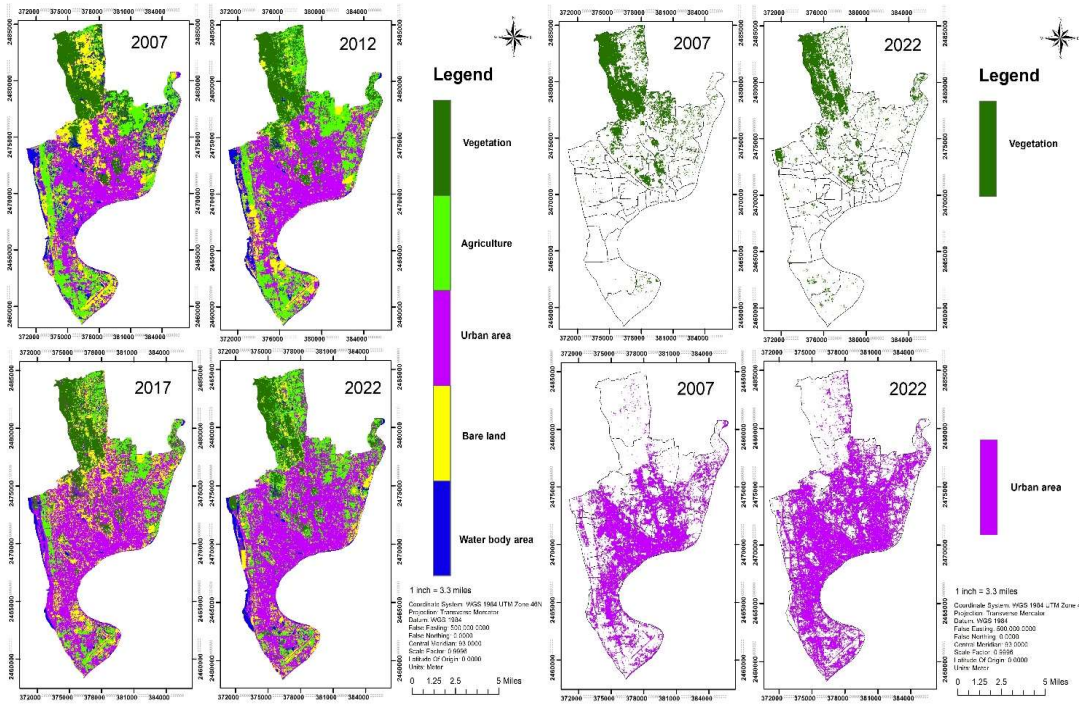

Fig. 5: Land use and land cover map from and the changes in vegetation and urban area from 2007 to 2022.

There was a noticeable change in the land use and land cover of the Chattogram region between 2007 and 2022. Analyses of change detection demonstrated that several land use and land cover categories had undergone considerable changes. In 2007, urban land took up 34.77% of the research area's land area, followed by agricultural land (21.46% of the area), bare land (18.95% of the area), and vegetation (17.77%). Water bodies made up 7.05% of the study area's land area. The findings showed that the percentage of vegetation cover and bare land decreased to 3.85% and 9.67%, respectively. However, Chattogram City's urban area drastically increased to 51.51% of the total area (Table 1).

Indicative Changes in LULC by 2037

By examining two qualitative land uses from two distinct periods, Markov creates a transition matrix or a transition area matrix. For this study, 15 years of data from 2007 to 2022 (Table 2) was used. More recent land cover usage is represented by the column, whereas older land cover use is represented by the rows. Agriculture, bare terrain, urban, vegetation, and water bodies are represented here in chronological order by the categories. Here, the Markov analysis used the matrix to forecast how the land cover will be used in 2037 (Islam & Ahmed 2011).

According to the transition matrix, the probability of change for agricultural land is that 39.29% of the current agricultural area will remain the same in 2037. Of the current area, 11.19% may become bare land, 41.28% may become urban areas, 5.97% may become vegetation, and 2.27 percent may become water body areas (Table 2). 19.64 percent of the current bare land area is likely to remain unchanged in 2037, which would represent no change in the bare land area. Currently, agriculture can occupy 28.20 percent of the land, whereas urban uses can occupy 41.20 percent, vegetation can occupy 8.36 percent, and water bodies can occupy 2.59 percent (Table 2). Similar to this, in 2037, 86% of the currently developed urban land will still be there, with 4.53% of it being bare land, 5.15 % being used for agriculture, 1.49% being covered in vegetation, and 2.56% being a body of water. In 2037, it is anticipated that 53.97 percent of the area's vegetation cover will remain the same, while 15.56 percent of it may become urban, 4.55 percent could turn into bare ground, 25.57 percent could be used for agriculture, and 0.35 percent could turn into a body of water (Table 2). In terms of the water body area, there will be no change of 24.91 percent in 2037. However, 12.74 percent may be covered by vegetation, 41.54 percent by urban, 4.17 percent by bare land, and 16.64 percent by agriculture (Table 2).

Relationship between NDVI and LST

Fig. 6 shows the relationship between NDVI and LST. It has been demonstrated that the NDVI and surface temperature have a negative correlation. This is a blatant indication that the LST and NDVI have a high and unfavorable correlation. As a result, the land surface temperature is higher in areas with less vegetation. Fig. (6) shows that the area's temperature regime has been significantly impacted by changes in land use. However, compared to other locations, such as city areas, the vegetative area had a lower temperature. In comparison to urban green spaces such as parks and agricultural fields, LST values were comparatively greater in urban areas with no vegetation cover. Because there is a negative association between NDVI and LST, areas with lower NDVI values have higher land surface temperatures, whereas areas with higher NDVI values have lower land surface temperatures (Gorgani et al. 2013). The value of the NDVI in 2007 ranged from +0.6 to -0.25, with a negative value indicating lesser vegetation cover (Table 3), which typically indicates places with water cover. By looking at Fig. 6, it is clear that this range was true in 2007. The LST map for 2007 displays the same information, indicating that the maximum LST was 38°C and the minimum LST was 24.5°C (Table 3). It is evident from the 2007 co-relationship diagram that NDVI value decreases with high LST value and increases with low LST value. The NDVI value was 0.289 in the trend line of correlation (Fig. 6) when the LST value was close to 25°C, but it constantly declined with higher LST values, as can be seen when the LST value was close to 38°C, and the NDVI value was negative at -0.075. That indicates that in 2007, the trend line unmistakably demonstrated a negative association between NDVI and LST (Fig. 6). With a slightly different NDVI and LST value for the year 2012, it was essentially a

Table 2: Probability of changes in the year 2037 land cover (prediction) using transition matrix.

Class	Agriculture	Bare land	Urban	Vegetation	Water Body	Grand Total
Agriculture	39.29%	11.19%	41.28%	5.97%	2.27%	100%
Bare land	28.20%	19.64%	41.20%	8.36%	2.59%	100%
Urban	5.15%	4.53%	86.28%	1.49%	2.56%	100%
Vegetation	25.57%	4.55%	15.56%	53.97%	0.35%	100%
Waterbody	16.64%	4.17%	41.54%	12.74%	24.91%	100%

Markov's prediction of land use change in the next 15 years

Table 3: Retrieved statistics of LST (°C) and NDVI values from 2007-2022.

	LST				NDVI			
	2022	2017	2012	2007	2022	2017	2012	2007
Maximum	42.0361	37.755	37.2995	38.0009	0.608817	0.564	0.447368	0.6
Minimum	24.7868	20.2609	20.2609	24.5451	-0.17095	-0.15216	-0.28571	-0.25
Mean	33.41145	29.00795	28.7802	31.273	0.218932	0.205919	0.080827	0.175
Standard Deviation	12.1971	12.3702	12.04811	9.514687	0.551381	0.506403	0.518367	0.601040764

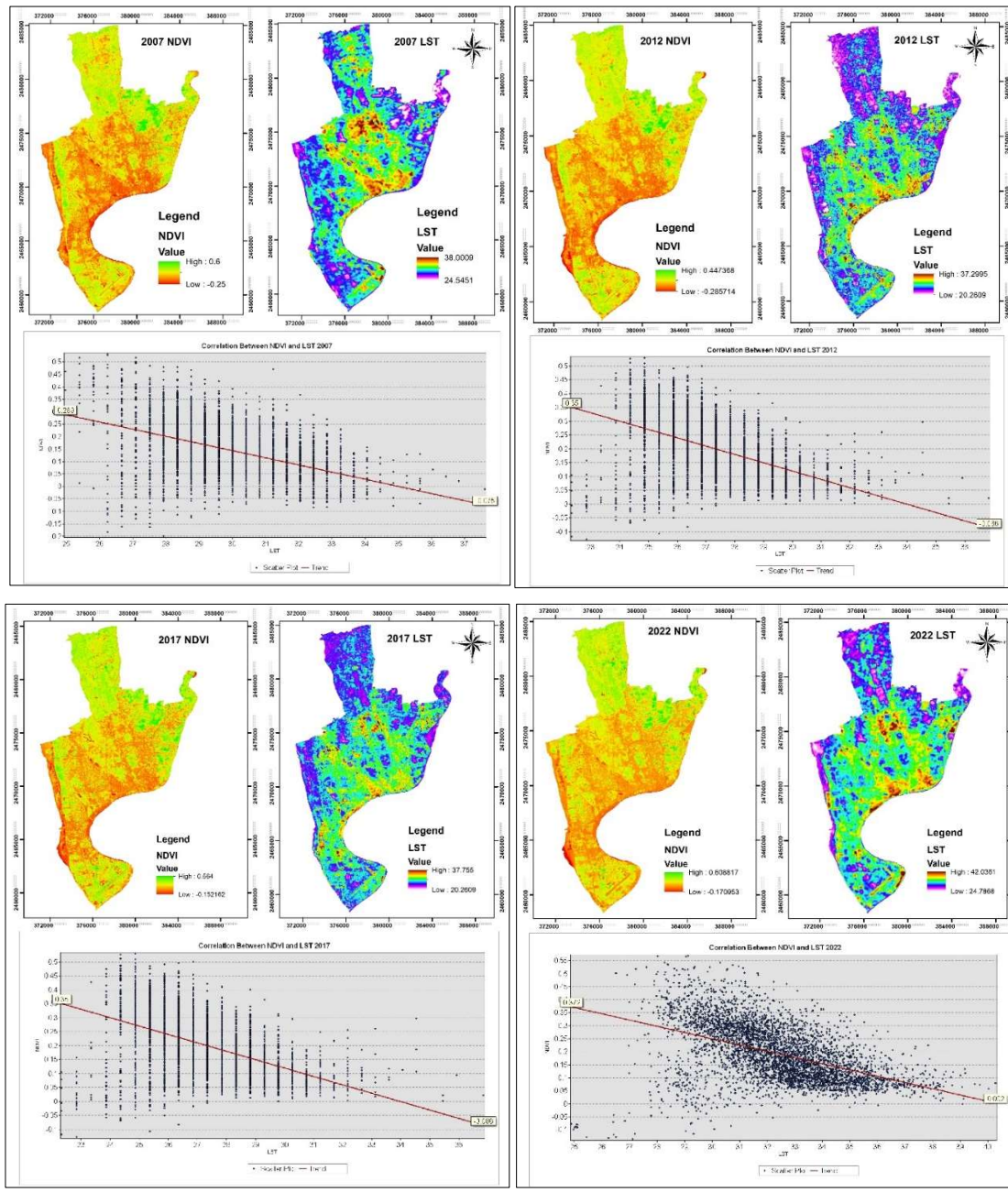

Fig. 6: Correlation of LST and NDVI from the year 2007 to 2022.

reflection of the year 2007. The trend line for 2012 shows a similar outcome to that of 2007, where the NDVI value is 0.237 while the LST is close to 22°C but continuously decreases as the LST increases (Fig. 6). The NDVI value is -0.221 when the LST value is near 35°C. This clearly illustrates the conflict between the NDVI and LST. This implies the tendency of inverse relationships between NDVI and LST where the increase of NDVI values fits the decrease of LTS values and vice versa. In the same way, in 2017 the relationship showed a negative trend line between NDVI and LST. In 2017 the highest NDVI was +0.56, and the lowest NDVI was -0.15, while the maximum LST and lowest LST values were 37.7°C and 20.26°C, respectively (Table 3). The trend line indicated that less vegetation will be present if the LST has a higher value when the relationship between them is taken into account. When the LST was close to 37°C, the NDVI value was negative (-0.086), indicating the absence of vegetation, as it was in 2017 when the NDVI value was 0.35 on the trendline (Fig. 6). In 2022 the result was quite similar as the correlation was negative. In 2022, the higher NDVI value was +0.60, and -0.17 was the lowest NDVI score. The highest LST and lowest LST in 2022 were 42.03°C and 24.78°C, respectively (Fig. 6). The trendline indicated that less vegetation will be present if the LST has a higher value when the relationship between them is taken into account. The NDVI had a low value of 0.02 when the LST was close to 41°C, indicating very little vegetation, but it had a high value of +0.37 when the LST was close to 25°C (Fig. 6).

DISCUSSION

Gain-loss and net change estimation from the four temporal periods of 2007 to 2012, 2012 to 2017, 2017 to 2022, and 2007 to 2022 were detected using the continuous analysis of LULC. Nearly all of the land use land cover classes displayed gains and losses. Gain and loss graphs for various purposes (Fig. 7) were made per category to aid in understanding. From the transition matrix (Table 4) it can be identified that lands from different categories have changed with time. The area, which was covered by water in 2007, transformed into an urban area, which is about 472 ha of land. Also, there is a significant change has been shown in the vegetation area which has been converted into an urban area in the last 15 years. About 470 ha of land has been converted from a vegetation area to an urban buildup area; also, about 772 ha of land has been converted into agricultural land in the last 15 years in Chattogram city. The conversion of vegetation land to bare land is also alarming for the overall environment of Chattogram City. About 137 ha of land has been converted from vegetation to bare land. Because of the gain of urban area and loss of vegetation area, it is significantly impacting the thermal environment of the city. The Land Surface Temperature (LST) and NDVI both show their characteristics because of these changes (Table 5). ArcGIS 10.4 image processing software is used to display the LST and NDVI images of Chattogram side by side to better comprehend the LST and NDVI pattern. The spatial distribution of the urban thermal environment and vegetation cover in Chattogram City is depicted in Fig. 8 in an instructive manner. The urban area of Chattogram has a higher LST than the surrounding area of vegetation and agricultural land. It is evident that non-porous materials, such as metal, asphalt, and concrete, which are used to construct city structures and main transportation corridors, contribute to greater temperatures (Hoehne et al. 2022). Water bodies, agricultural areas, and vegetation, on the other hand, all have lower temperatures. In the NDVI image (Fig. 8), the values are the exact opposite. Due to the lack of vegetation, built-up or core city regions have low NDVI values, as do water body locations. Because green biomass is present at relatively high levels, high values are found in agriculture, vegetation, and green land areas (Prashar et al. 2022).

Regarding LST, the phenomenon that LST values are disproportionately greater in the built-up or core urban area than in the suburbs makes the impact of the urban thermal environment clear. Except for a few open spaces, NDVI values in the built-up or core city region are significantly lower than in the suburbs. When comparing LST and NDVI, one discovers that their respective changing trends are completely at odds (Table 5). LST values are typically high where the main city area or buildup area is situated, while they are typically low where bodies of water and green space are present. The green space is where the NDVI peaks arise. LST and NDVI typically exhibit a clear inverse association. On the other hand, Chattogram's urban form and urban sprawl are intimately tied to the shifting trends of LST or NDVI.

Table 5 presents the regression functions and correlation coefficient (R2), which gauges the potency of linear regression to show the relationship between LST and NDVI for each LULC type. NDVI and LST of all LULC categories, except water bodies, showed a substantial inverse association. For every year the greatest negative regression slope was indicated by "Urban area," while the shallowest negative regression slope was revealed by "Vegetation area." Fig. 8 illustrates that the NDVI and LST association was consistently negative except water body area. The NDVI reduced as LST grew at all-time intervals due to having a negative connection, and this association demonstrated that when a lower Vegetation Level was present, the LST increased (Table 5). In other words, higher Vegetation Levels

Table 4: Land Use Land Cover Transition Matrix 2007-2022 in Hectors.

	Land cover class 2022					
	Land Class	Agriculture	Bare land	Urban	Vegetation	Water Body	Grand Total
Land cover class 2007	Agriculture	1431.744195	407.898234	1504.122069	217.562777	82.592654	3643.919929
	Bare land	893.989644	622.767495	1306.324578	265.116518	82.140167	3170.338402
	Urban	307.313042	270.381518	5153.086372	88.993963	152.719009	5972.493904
	Vegetation	772.824363	137.596243	470.26625	1631.57592	10.622077	3022.884852
	Waterbody	189.196549	47.430983	472.239674	144.855487	283.202797	1136.92549
	Grand Total	3595.067793	1486.074473	8906.038943	2348.10466	611.276704	16946.56258

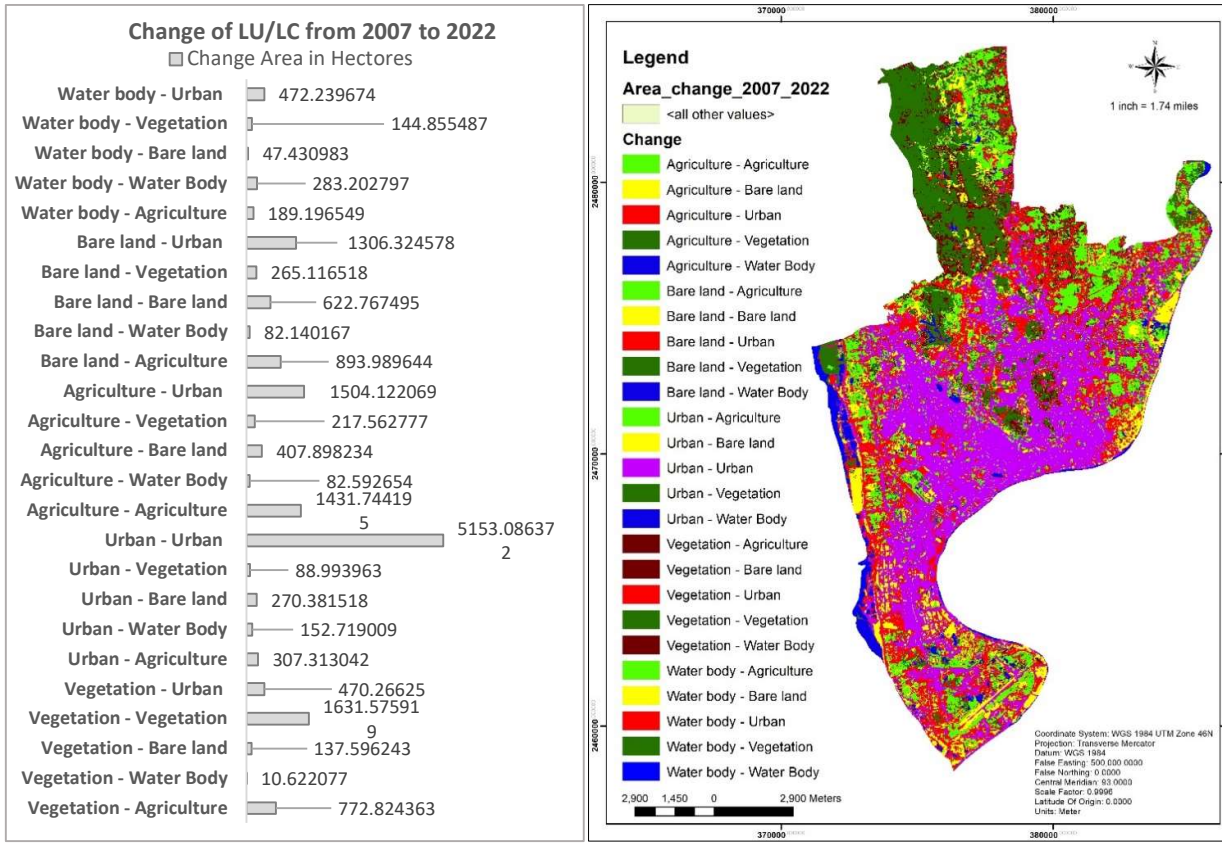

Fig. 7: Changes in Land cover in each category from 2007 to 2022.

caused lower LST while lower vegetation levels caused higher LST (Fig. 8). So if the vegetation decreases with time in the Chattogram region, a significant amount of LST will increase, which is usually responsible for creating an Urban heat island that also has a direct impact on the overall temperature of the city (Roy et al. 2020). According to (Farzana et al. 2022), a city's heat island can also have an impact on precipitation, which is a problem for Chattogram City.

The swift growth of the population in the urban area of Chattogram City and its changing patterns of land use and land cover (LULC) has brought about tremendous changes in the urban thermal environment –that is, the urban heat islands (UHI) phenomenon is becoming increasingly prevalent. With the growth of the built-up areas, especially those where trees and farms are cleared, the UHI intensity increases, which in turn has far-reaching consequences on health, diversity, and energy usage. Citing previous studies, it can be said these increasing UHI effects worsen heat stress and the associated health risks, especially during heat waves which are very dangerous to certain people, such as the aged and those with underlying illnesses (Liu et al. 2021, Wang et al. 2021). With the growing infrastructure in Chattogram City, for example, there is a loss of vegetation and enhancement of pavements. As a result, the capacity of the land to cool down using

Table 5: LST and NDVI Relationship by LULC Type.

Class (2007-2022)	2022	2017	2012	2007
	Regression function and (R^2)	Regression function and (R^2)	Regression function and (R^2)	Regression function and (R^2)
Vegetation	y = -10.502x + 32.449 R² = 0.1912	y = -7.9417x + 27.748 R² = 0.1925	y = -3.8895x + 25.705 R² = 0.1143	y = -5.1192x + 29.643 R² = 0.1151
Agriculture	y = -12.517x + 34.941 R² = 0.5495	y = -6.8163x + 28.026 R² = 0.5096	y = -6.3522x + 27.371 R² = 0.4693	y = -11.12x + 31.164 R² = 0.4159
Urban	y = -29.924x + 37.13 R² = 0.2255	y = -11.624x + 30.041 R² = 0.1868	y = -12.469x + 27.854 R² = 0.1794	y = -15.409x + 32.227 R² = 0.229
Bare land	y = -19.346x + 38.531 R² = 0.5969	y = -2.9813x + 29.199 R² = 0.0397	y = -5.6523x + 27.541 R² = 0.0034	y = -12.806x + 33.853 R² = 0.314
Water area	y = 8.6653x + 28.799 R² = 0.1108	y = 1.1331x + 23.87 R² = 0.0021	y = 7.8215x + 25.113 R² = 0.2422	y = 5.4723x + 27.463 R² = 0.0552

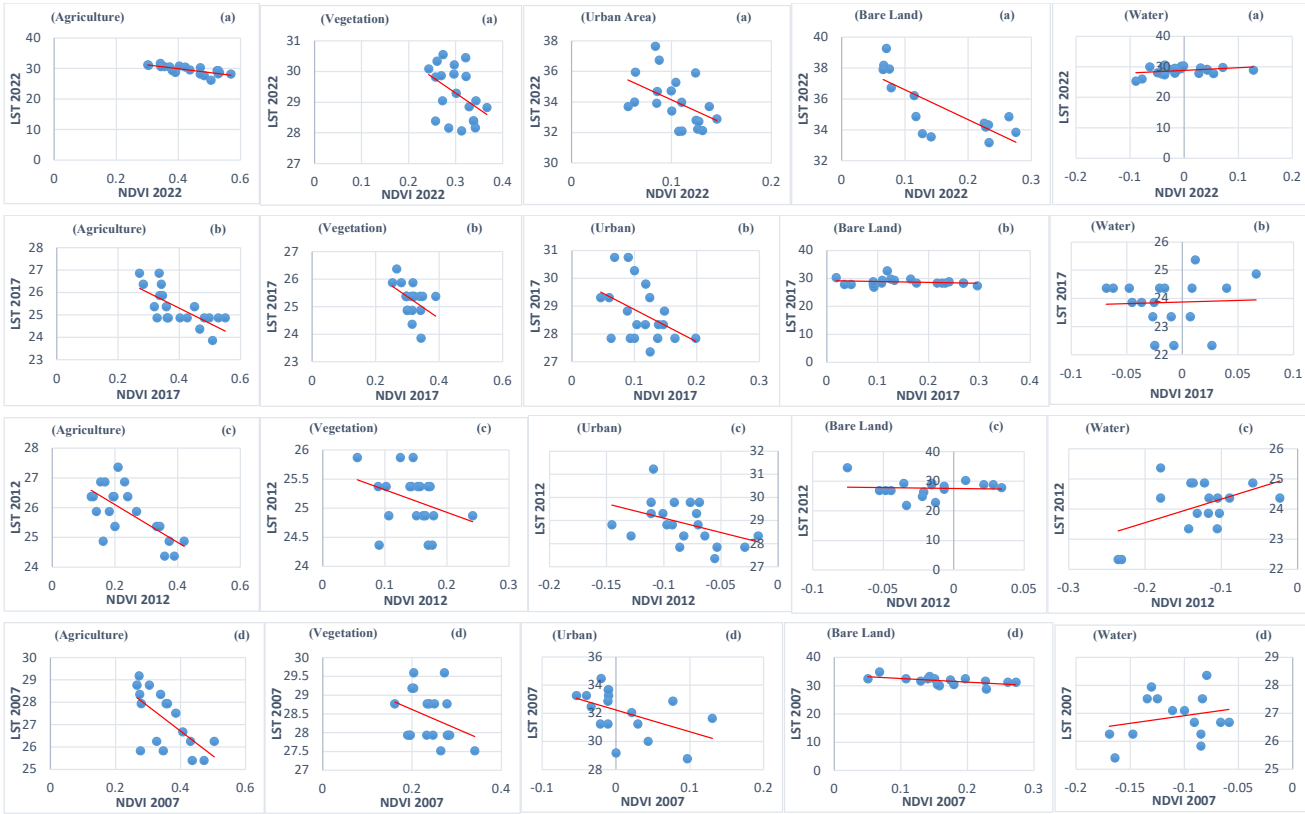

Fig. 8: LST and NDVI relationship by LULC Type for the years 2022 (a), 2017 (b), 2012 (c), 2007 (d).

an efficient natural process known as evapotranspiration reduces. There is a body of literature that supports the view that such a process is very important in controlling surface temperatures in other cities that have undergone similar transformations (Atasoy 2020, Zhou et al. 2022). Extreme weather conditions attributed to urban surfaces not only mean hotter temperatures but also prolonged hot days and warm nights (Wang et al. 2021).

The impact on the environment goes further than just human well-being. Urban biodiversity is especially sensitive to the higher temperatures resulting from the urban heat island effect. Species twice as rapidly as climate-adjusting species pose a risk of extinction or decline in numbers (Kong et al. 2021). The intensified UHI effect also increases the energy consumption demand for buildings, especially air conditioning. Also, this may lead to high-energy use and emissions, which contribute to the problem of combating urban ecological pollution (Dudorova & Belan 2022, Liu et al. 2021). Overall, the results from Chattogram City are consistent with worldwide observations, where uncontrolled

urban development contributes significantly to increased UHI effects, which presents great threats to human health, the environment as well as energy utilization. Addressing these negative effects requires strategic urban development and active measures to mitigate the effects including increasing urban vegetation as well as the use of energy-effective technologies (Jusuf et al. 2019, Kong et al. 2021).

CONCLUSIONS

The analysis shows that there have been significant changes in land use and land cover in the Chattogram City region during the past 15 years. This study also illustrates how the study area's urban heat island is distributed spatially and how land surface temperature fluctuates over time. For four separate years 2007, 2012, 2017, and 2022 the study has determined the land surface temperature and the urban heat island zone. Due to changes in land use and land cover, there have been observed variations in land surface temperature and urban heat islands, which have altered radiant surface temperatures and ultimately produced urban heat island zones. In the Chattogram City Area, the urban area had the largest land cover (34.77 percent of the entire study area) in 2007, and it rapidly rose in 2012, 2017, and 2022. In 2022, the urban area became the CMA's main and significant land cover, accounting for 51.51 percent of the entire study area, while the covering of dominating vegetation declined by 654.39 ha. The land surface temperature in Chattogram City significantly increased between 2007 and 2022 as a result of the shift in land usage. Rooftop gardening and plantations might help restore some of the lost green space that has been lost over the previous few decades, which may help to regulate the current level of UHI.

Additionally, rooftop gardening and tree planting can lower the temperature of the city of Chattogram's surface as well. Both of the mayors of the city corporations in Dhaka, the capital of Bangladesh, have promised a 10% holding tax discussion to promote rooftop gardening. Even if only half of the structures in Chattogram allowed for rooftop gardening, it would still be good for the city's ecosystem. The rooftop tree plantation and gardening plan in Chattogram City may be difficult to accomplish due to a lack of awareness, policy, and management. However, action must be taken in the Chattogram City area for a safe and environmentally friendly future.

ACKNOWLEDGMENTS

The authors are grateful and give thanks for this work being supported by the faculty and officials of the Department of Environmental Science and Disaster Management (ESDM), Daffodil International University (DIU).

REFERENCES

Abburu, S. and Golla, S.B., 2015. Satellite image classification methods and techniques: A review. *International Journal of Computer Applications*, 119(8), pp.1-10.

Ahmed, B., 2011. Urban land cover change detection analysis and modeling spatio-temporal growth dynamics using remote sensing and GIS techniques: A case study of Dhaka, Bangladesh. *Journal of Geospatial Science and Technology*, 5(2), pp.45-60.

Atasoy, M., 2020. Assessing the impacts of land-use/land-cover change on the development of urban heat island effects. *Environment, Development and Sustainability*, 22(8), pp.7547–7557. [DOI]

Avdan, U. and Jovanovska, G., 2016. Algorithm for automated mapping of land surface temperature using LANDSAT 8 satellite data. *Journal of Sensors*, 2016, pp.1-12.

Baik, H.S., Jeong, HS. and Abraham, D.M., 2006. Estimating transition probabilities in Markov chain-based deterioration models for management of wastewater systems. *Journal of Water Resources Planning and Management*, 132(1), pp.15–24.

Barsi, J.A., Schott, J.R., Hook, S.J., Raqueno, N.G., Markham, B.L. and Radocinski, R.G., 2014. Landsat-8 thermal infrared sensor (TIRS) vicarious radiometric calibration. *Remote Sensing*, 6(11), pp.11607–11626.

BBS, 2011. *Bangladesh Bureau of Statistics, Ministry of Planning*. Govt. of Bangladesh, Dhaka.

Chander, G., Markham, B.L. and Helder, D.L., 2009. Summary of current radiometric calibration coefficients for Landsat MSS, TM, ETM+, and EO-1 ALI sensors. *Remote Sensing of Environment*, 113(5), pp.893–903.

Curran, P., 1980. Multispectral remote sensing of vegetation amount. *Progress in Physical Geography*, 4(3), pp.315–341.

Dudorova, N.V. and Belan, B.D., 2022. The energy model of urban heat island. *Atmosphere*, 13(3). [DOI]

Farzana, R., Tabassum, A., Mannan, Md.A. and Karunatillake, S., 2022. Assessment of UHI and its long-term impact on temperature, precipitation, and evapotranspiration for the major cities in Bangladesh. *SSRN Electronic Journal*. [DOI]

Fatemi, M. and Narangifard, M., 2019. Monitoring LULC changes and its impact on the LST and NDVI in District 1 of Shiraz City. *Arabian Journal of Geosciences*, 12(4), pp.1–12.

Gaonkar, V.G., Nadaf, F.M. and Kapale, V., 2024. Mapping and quantifying integrated land degradation status of Goa using geostatistical approach and remote sensing data. *Nature Environment & Pollution Technology*, 23(1), pp.1–15.

Gazi, M., Rahman, M., Uddin, M. and Rahman, F.M., 2021. Spatio-temporal dynamic land cover changes and their impacts on the urban thermal environment in the Chittagong metropolitan area, Bangladesh. *GeoJournal*, 86(5), pp.2119–2134.

Gorgani, S.A., Panahi, M. and Rezaie, F., 2013. The relationship between NDVI and LST in the urban area of Mashhad, Iran. *International Conference on Civil Engineering Architecture & Urban Sustainable Development*, 27&28 November, 51, pp.1–10.

Hassan, M.M. and Nazem, M.N.I., 2016. Examination of land use/land cover changes, urban growth dynamics, and environmental sustainability in Chittagong City, Bangladesh. *Environment, Development and Sustainability*, 18(3), pp.697–716.

Hoehne, C.G., Chester, M.V., Sailor, D.J. and King, D.A., 2022. Urban heat implications from parking, roads, and cars: A case study of Metro Phoenix. *Sustainable and Resilient Infrastructure*, 7(4), pp.272–290. [DOI]

Hokao, K., Phonekeo, V. and Srivanit, M., 2012. Assessing the impact of urbanization on urban thermal environment: A case study of Bangkok Metropolitan. *International Journal of Applied*, 2(7), pp.1–12.

Islam, M.S. and Ahmed, R., 2011. Land use change prediction in Dhaka

City using GIS-aided Markov chain modeling. *Journal of Life and Earth Science*, 6, pp.81–89.

Jabbar, H.K., Hamoodi, M.N. and Al-Hameedawi, A.N., 2023. Urban heat islands: A review of contributing factors, effects and data. *IOP Conference Series: Earth and Environmental Science*, 1129(1), 012038. [DOI]

Jensen, J.R., 1996. *Introductory Digital Image Processing: A Remote Sensing Perspective*. 2nd ed. Prentice-Hall Inc.

Jiménez-Muñoz, J.C., Sobrino, J.A., Gillespie, A., Sabol, D. and Gustafson, W.T., 2006. Improved land surface emissivities over agricultural areas using ASTER NDVI. *Remote Sensing of Environment*, 103(4), pp.474–487.

Jiménez-Muñoz, J.C., Sobrino, J.A., Plaza, A., Guanter, L., Moreno, J. and Martínez, P., 2009. Comparison between fractional vegetation cover retrievals from vegetation indices and spectral mixture analysis: Case study of PROBA/CHRIS data over an agricultural area. *Sensors*, 9(2), pp.768–793.

Jusuf, S.K., Ignatius, M., Hien, W.N. and Akbari, H., 2019. Editorial: Urban heat island (UHI) and its mitigation through urban planning, design, and landscaping. *Architectural Science Review*, 62(1), pp.1–2. [DOI]

Karakuş, C.B., 2019. The impact of land use/land cover (LULC) changes on land surface temperature in Sivas city center and its surroundings and assessment of urban heat island. *Asia-Pacific Journal of Atmospheric Sciences*, 55(4), pp.669–684.

Kavitha, A.V., Srikrishna, A. and Satyanarayana, Ch., 2021. A review on detection of land use and land cover from an optical remote sensing image. *IOP Conference Series: Materials Science and Engineering*, 1074(1), 012002. [DOI]

Kirkpatrick, J., 2024. A big history of land clearance and deforestation. *Journal of Big History*, 7(3), pp.1–18. [DOI]

Kong, J., Zhao, Y., Carmeliet, J. and Lei, C., 2021. Urban heat island and its interaction with heatwaves: A review of studies on mesoscale. *Sustainability (Switzerland)*, 13(19). [DOI]

Lillesand, T., Kiefer, R.W. and Chipman, J., 2015. *Remote Sensing and Image Interpretation*. John Wiley & Sons.

Liu, B., Xie, Z., Qin, P., Liu, S., Li, R., Wang, L., Wang, Y., Jia, B., Chen, S., Xie, J. and Shi, C., 2021. Increases in anthropogenic heat release from energy consumption lead to more frequent extreme heat events in urban cities. *Advances in Atmospheric Sciences*, 38(3), pp.430–445. [DOI]

Lo, C.P. and Quattrochi, D.A., 2003. Land-use and land-cover change, urban heat island phenomenon, and health implications. *Photogrammetric Engineering & Remote Sensing*, 69(9), pp.1053–1063.

Long, H., Tang, G., Li, X. and Heilig, G.K., 2007. Socio-economic driving forces of land-use change in Kunshan, the Yangtze River Delta economic area of China. *Journal of Environmental Management*, 83(3), pp.351–364.

Markham, B.L. and Barker, J.L., 1985. Spectral characterization of the Landsat Thematic Mapper sensors. *International Journal of Remote Sensing*, 6(5), pp.697–716.

Meyer, W.B., 1995. Past and present land use and land cover in the U.S.A. *Consequences: The Nature and Implications of Environmental Change*, 1(1), pp.XX–XX.

Mia, B., Bhattacharya, R. and Woobaidullah, A.S.M., 2017. Correlation and monitoring of land surface temperature, urban heat island with land use-land cover of Dhaka city using satellite imageries. *International Journal of Research in Geography*, 3(1), pp.10–20.

Mia, M.A., Nasrin, S., Zhang, M. and Rasiah, R., 2015. Chittagong, Bangladesh. *Cities*, 48, pp.31–41.

Pasha, A.B.M.K., Chowdhury, A.H., Hussain, A., Rahman, M., Mozumder, S. and Fuente, J.A.D., 2023. Identification of the ecosystem services and plant diversity in Ramna Park Dhaka. *International Journal of Environmental Studies*, 20(2), pp.65-89.

Pasha, A.B.M.K., Mozumder, S., Bhuiyan, M.A.H. and Parveen, M., 2018. Monitoring land use and land cover changes of Dhaka City: A remote sensing and GIS-based analysis. *International Journal of Geospatial Studies*, 10(2), pp.45–60.

Pathirana, A., Denekew, H.B., Veerbeek, W., Zevenbergen, C. and Banda, A.T., 2014. Impact of urban growth-driven land use change on microclimate and extreme precipitation—A sensitivity study. *Atmospheric Research*, 138, pp.59–72.

Prashar, Y., Sharma, R., Kumar, S., Hassan, S.S. and Pateriya, B., 2022. Analyzing the impact of built-up and green spaces on land surface temperature with satellite images in Jalandhar Smart City. *International Journal on Environmental Sciences*, 13(2), pp.99–106. [DOI]

Qian, Y., Chakraborty, T.C., Li, J., Li, D., He, C., Sarangi, C., Chen, F., Yang, X. and Leung, L.R., 2022. Urbanization impact on regional climate and extreme weather: Current understanding, uncertainties, and future research directions. *Advances in Atmospheric Sciences*, 39(6), pp.819–860. [DOI]

Qin, Z., Karnieli, A. and Berliner, P., 2001. A mono-window algorithm for retrieving land surface temperature from Landsat TM data and its application to the Israel-Egypt border region. *International Journal of Remote Sensing*, 22(18), pp.3719–3746.

Ritchie, H. and Roser, M., 2018. *Urbanization*. Our World in Data.

Ross, S.M., 2014. *Introduction to Probability Models*. Academic Press.

Roy, S., Pandit, S., Eva, E.A., Bagmar, Md.S.H., Papia, M., Banik, L., Dube, T., Rahman, F. and Razi, M.A., 2020. Examining the nexus between land surface temperature and urban growth in Chattogram Metropolitan Area of Bangladesh using long-term Landsat series data. *Urban Climate*, 32, 100593. [DOI]

Saraswat, A., Pipralia, S. and Kumar, A., 2024. Exploring the application of ecosystems approach to urban planning. *International Review for Spatial Planning and Sustainable Development*, 12(2), pp.28–42. [DOI]

Shahbaz, M., Guergachi, A., Noreen, A. and Shaheen, M., 2012. Classification by object recognition in satellite images by using data mining. *Proceedings of the World Congress on Engineering*, 1, pp.4–6.

Singh, G. and Singh, S.K., 2023. Evapotranspiration over the Indian region: Implications of climate change and land use/land cover change. *Nature Environment and Pollution Technology*, 22(1), pp.211–219.

Sobrino, J.A. and Raissouni, N., 2000. Toward remote sensing methods for land cover dynamic monitoring: Application to Morocco. *International Journal of Remote Sensing*, 21(2), pp.353–366.

Sobrino, J.A., Jiménez-Muñoz, J.C. and Paolini, L., 2004. Land surface temperature retrieval from LANDSAT TM 5. *Remote Sensing of Environment*, 90(4), pp.434–440.

Statistics, 2011. Bangladesh Bureau of Statistics, Statistics and Informatics Division (SID), Ministry of Planning, Parishankhan Bhaban, E-27/A, Agargaon, Dhaka-1207

Tan, K.C., Lim, H.S., MatJafri, M.Z. and Abdullah, K., 2010. Landsat data to evaluate urban expansion and determine land use/land cover changes in Penang Island, Malaysia. *Environmental Earth Sciences*, 60(7), pp.1509–1521.

Thomas, G.S., Liu, Y. and Mwanga, N., 2024. Exploring the environmental effects of urbanization in Monrovia. *European Journal of Theoretical and Applied Sciences*, 2(3), pp.1117–1130. [DOI]

Tyagi, S.K., Kumar, V., Kumar, K. and Kumar, D., 2023. Environmental health quality and the consequences of urbanization: A review. *International Journal of Advances in Agricultural Science and Technology*, 10(5), pp.13–23. [DOI]

Vaiphasa, C., Piamduaytham, S., Vaiphasa, T. and Skidmore, A.K., 2011. A normalized difference vegetation index (NDVI) time-series of idle agriculture lands: A preliminary study. *Engineering Journal*, 15(1), pp.9–16.

Verburg, P.H., Chen, Y., Soepboer, W. and Veldkamp, A., 2000. GIS-based modeling of human-environment interactions for natural resource management. *Proceedings of the 4th International Conference on Integrating GIS and Environmental Modeling: Problems, Prospects and Research Needs*, Canada, pp.1–13.

Wang, J., Chen, Y., Liao, W., He, G., Tett, S.F.B., Yan, Z., Zhai, P., Feng, J., Ma, W., Huang, C. and Hu, Y., 2021. Anthropogenic emissions and urbanization increase risk of compound hot extremes in cities. *Nature Climate Change*, 11(12), pp.1084–1089. [DOI]

Winston, W.L. and Goldberg, J.B., 2004. *Operations Research: Applications and Algorithms*. 3rd ed. Thomson Brooks/Cole Belmont.

Xu, H. and Chen, B., 2004. Remote sensing of the urban heat island and its changes in Xiamen City of SE China. *Journal of Environmental Sciences*, 16(2), pp.276–281.

Zhou, D., Xiao, J., Frolking, S., Zhang, L. and Zhou, G., 2022. Urbanization contributes little to global warming but substantially intensifies local and regional land surface warming. *Earth's Future*, 10(5), pp.1–19. [DOI]